ARTICLES
PUBLISHED ONLINE: 31 AUGUST 2015 | DOI: 10.1038/NNANO.2015.190
nature nanotechnology

Routing of individual polymers in designed patterns

Jakob Bach Knudsen[1,2], Lei Liu[1†], Anne Louise Bank Kodal[1,2], Mikael Madsen[1,2], Qiang Li[1], Jie Song[1], Johannes B. Woehrstein[3,4], Shelley F. J. Wickham[3], Maximilian T. Strauss[3,4], Florian Schueder[3], Jesper Vinther[1,2], Abhichart Krissanaprasit[1], Daniel Gudnason[1], Anton Allen Abbotsford Smith[2], Ryosuke Ogaki[1], Alexander N. Zelikin[2], Flemming Besenbacher[1], Victoria Birkedal[1], Peng Yin[3,5], William M. Shih[3], Ralf Jungmann[3,4,5], Mingdong Dong[1*] and Kurt V. Gothelf[1,2*]

Synthetic polymers are ubiquitous in the modern world, but our ability to exert control over the molecular conformation of individual polymers is very limited. In particular, although the programmable self-assembly of oligonucleotides and proteins into artificial nanostructures has been demonstrated, we currently lack the tools to handle other types of synthetic polymers individually and thus the ability to utilize and study their single-molecule properties. Here we show that synthetic polymer wires containing short oligonucleotides that extend from each repeat can be made to assemble into arbitrary routings. The wires, which can be more than 200 nm in length, are soft and bendable, and the DNA strands allow individual polymers to self-assemble into predesigned routings on both two- and three-dimensional DNA origami templates. The polymers are conjugated and potentially conducting, and could therefore be used to create molecular-scale electronic or optical wires in arbitrary geometries.

Polymer materials exhibit a plethora of useful properties as plastics, paints, fabric, glues and so on, and some types of polymers also encompass advanced mechanical, optical and electrical properties. Conjugated polymers offer the electronic and optoelectronic properties of semiconductor and metallic materials and also maintain the mechanical flexibility, processability and chemical diversity of organic polymers[1,2]. Their properties derive from the extended π-conjugated backbone that allows anisotropic charge delocalization along the polymer and they have been applied for organic electronics[3,4], light-emitting diodes[5,6], solar cells[7] and sensors[8].

Single-molecule synthetic polymers are, however, studied rarely because of their tendency to fold and aggregate. In some instances, the optical properties of individual conjugated polymers have been studied by single-molecule techniques[9]. Scanning probe microscopy is used to characterize the elasticity and mechanical properties of individual polymers by adhesion of the polymer to both the tip and the surface[10,11]. Sometimes, the optical and electronic properties of individual conjugated oligomers and polymers have been characterized[12–19]. The main obstacle to exploiting fully the integration of single-molecule properties of polymers in functional nanodevices is our lacking ability to handle individual polymers and control their conformation[20].

Synthesis of the conjugated APPV-DNA polymer

Here we present the synthesis, characterization and controlled immobilization of a conjugated (2,5-dialkoxy)paraphenylene vinylene (APPV) brush polymer containing a nine nucleotide (nt) single-stranded DNA (ssDNA) that extends from the majority of the phenylene groups. Conjugated polymers that interact non-covalently with DNA and conjugates of a single or a few DNA strands have been investigated previously[14,21,22]. However, the present conjugated APPV-DNA polymer enables a precise immobilization to predesigned line patterns on DNA origami through complementary ssDNA that extends from the backbone of the polymer and the DNA origami. DNA origami is a method for the self-assembly of DNA nanostructures and the structures constitute a uniquely addressable molecular two-dimensional (2D) or 3D breadboard with nanoscale dimensions[23,24]. The structures have been utilized previously for the controlled immobilization of proteins[25], nanoparticles[26] and carbon nanotubes[27]. Through the recognition of specific DNA strands, we demonstrate successfully the control of the shape of the material that is immobilized on DNA origami by routing and bending of individual polymer wires in 2D and 3D.

The key step in the preparation of the APPV-DNA polymer is the synthesis of 9-mer oligonucleotides directly on the APPV polymer via automated oligonucleotide synthesis[28]. We prepared the dithiocarbamate precursor **3** (Fig. 1 and Supplementary Fig. 1) in seven steps from **1** for the construction of the polymer backbone[29]. Precursor **3** contains a tris(ethylene glycol) side chain terminated with a *tert*-butyldiphenylsilyl (TBDPS) group that serves to solubilize the polymer and protect the alcohol. Subsequent polymerization was performed by deprotonation with lithium bis(trimethylsilyl)amide (LHMDS) at 35 °C (ref. 30) (Fig. 1 and Supplementary Fig. 2). The initial polymer still contains dithiocarbamate groups, which are thermally eliminated to form the conjugated APPV polymer **4a** over two steps in yields that range from 61 to 66% (Supplementary Figs 3, 4 and 8, and Supplementary Tables 1–3).

After partial removal of the TBDPS moiety to liberate some of the OH groups while keeping the polymer in solution (Supplementary Figs 5–7), poly((APPV-TBDPS)-*ran*-(APPV-OH)) (**4b**) was immobilized on 2-deoxythymidine (dT)-preloaded controlled pore glass (CPG) (Supplementary Fig. 9). Immobilization was achieved

[1]Centre for DNA Nanotechnology, Interdisciplinary Nanoscience Center, iNANO, Aarhus University, Gustav Wieds Vej 14, 8000 Aarhus C, Denmark. [2]Department of Chemistry, Aarhus University, Langelandsgade, 140, 8000 Aarhus C, Denmark. [3]Wyss Institute for Biologically Inspired Engineering, Harvard University, 3 Blackfan Circle, Boston, Massachusetts 02115, USA. [4]Max Planck Institute of Biochemistry and Ludwig-Maximilians-Universität, Am Klopferspitz 18, 82152 Martinsreid, Munich, Germany. [5]Department of Systems Biology, Harvard Medical School, 200 Longwood Avenue, Warren Alpert Building, Boston, Massachusetts 02115, USA; [†]Present address: Institute of Advanced Materials, Jiangsu University, 301 Xuefu Road, 212013, China. *e-mail: dong@inano.au.dk; kvg@chem.au.dk

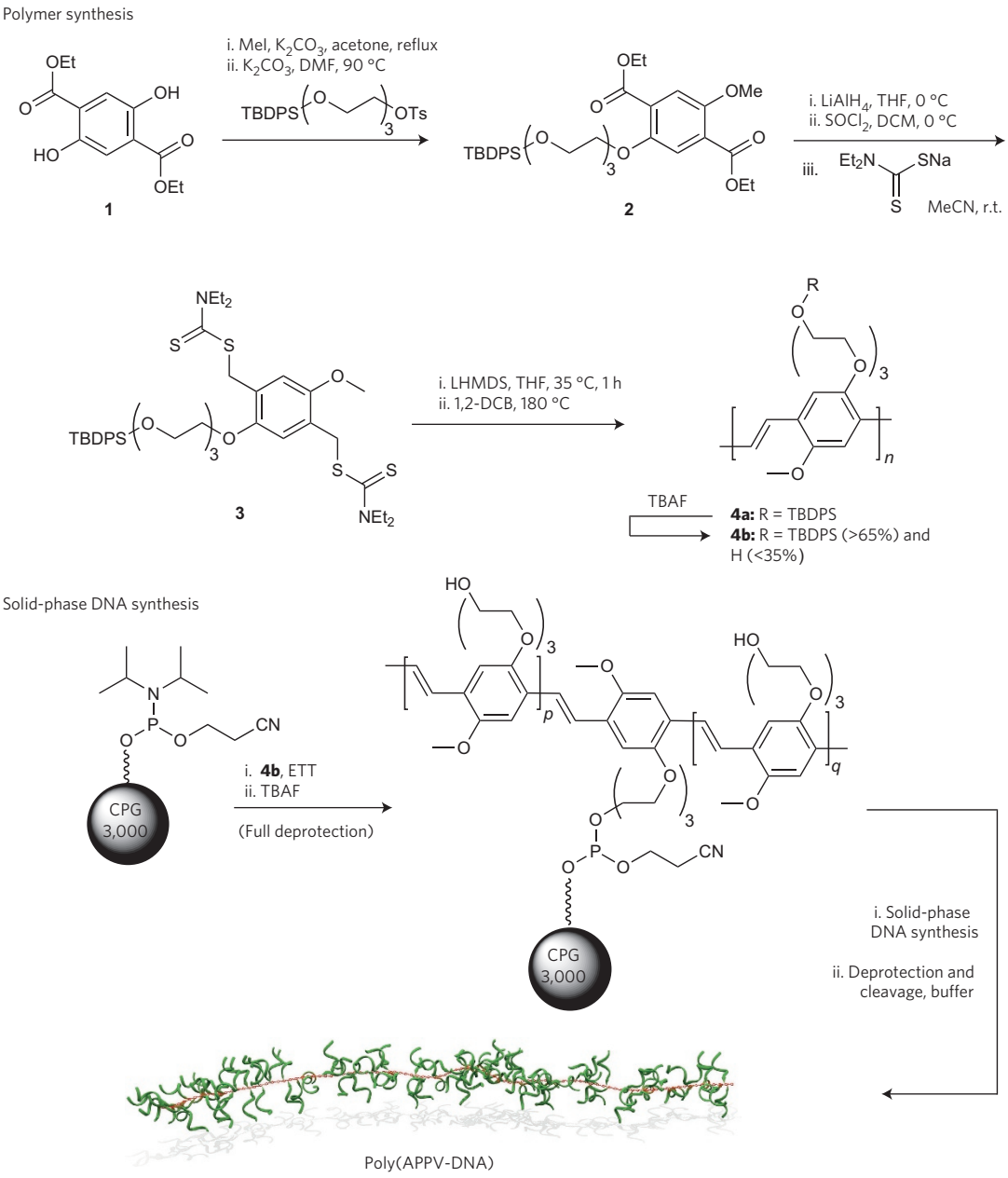

Figure 1 | Synthesis of poly(APPV-DNA). 1 (diethyl 2,5-dihydroxyterephthalate) is converted via **2** into the dithiocarbamate polymer precursor **3** followed by polymerization under alkaline conditions to give polymer **4a**. Partial TBDPS deprotection to give poly((APPV-TBDPS)-*ran*-(APPV-OH)) (**4b**) allows immobilization on a phosphoramidite-functionalized CPG support. After removal of the remaining protecting groups, 9 nt DNA sequences are synthesized on the polymer by automated DNA synthesis and finally poly(APPV-DNA) is deprotected and cleaved from the solid support. DCB, 1,2-dichlorobenzene; DCM, dichloromethane; DMF, dimethylformamide; ETT, ethyl thiotetrazole; TBAF, tetrabutylammonium fluoride.

by pre-activating the dT-CPG as a phosphoramidite followed by coupling with polymer **4b**. After immobilization the remaining TBDPS groups were removed, which liberated the majority of OH groups of the polymer. Using traditional automated solid-phase DNA synthesis, 9 nt DNA sequences were synthesized on the OH groups of the polymer[28,31]. After standard deprotection and cleavage from the solid support, the now fully water-soluble polymer was purified by size-exclusion chromatography.

Characterization of the polymer

The purified polymer samples were lyophilized and analysed by gel permeation chromatography (GPC), ultraviolet–visible (UV-vis) and fluorescence spectroscopy, X-ray photoelectron spectroscopy (XPS) and atomic force microscopy (AFM) (Supplementary Figs 10–12). The GPC analysis of the poly(APPV-DNA) indicated that the sizes of the polymer molecules ranged from around 340 kDa up to around 3,300 kDa (Supplementary Tables 4 and 5). Partial degradation of the polymer by cleavage into shorter pieces was observed during the purification and therefore it was not possible to obtain fractions of the polymer with high monodispersity. UV-vis characterization of poly(APPV-DNA) showed absorbance peaks at 260 nm and 545 nm, and the fluorescence spectra showed a broad fluorescent emission in the range 550–700 nm (Supplementary Figs 13 and 14). The fluorescence quantum yield of the poly(APPV-DNA) was determined to be 0.3 using Sulforhodomine 101 as a standard.

The elemental composition of the APPV-DNA polymer obtained by XPS suggests that it contains DNA strands on slightly

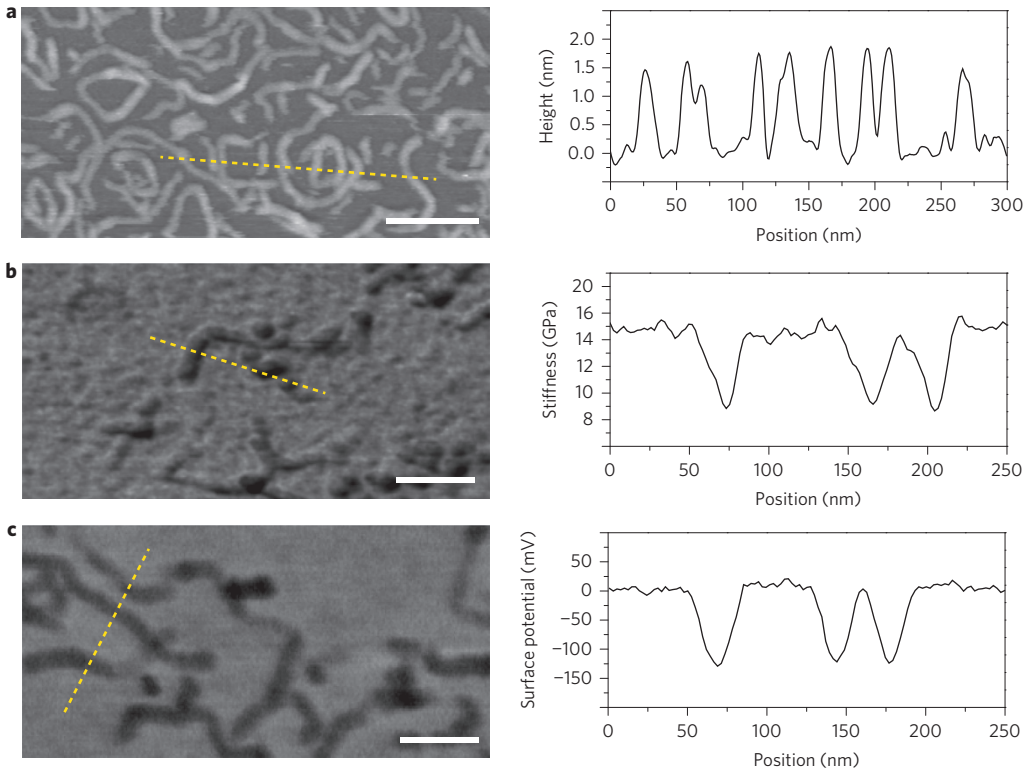

Figure 2 | AFM characterization of the physical properties of poly(APPV-DNA). a, The topography and height measurements of poly(APPV-DNA). **b**, The stiffness measurement of poly(APPV-DNA). **c**, The surface potential measurement of poly(APPV-DNA). Scale bars, 100 nm.

less than two-thirds of the phenylene units. The estimate is based on the content of P and N relative to C (Supplementary Table 6). The melting temperature of the APPV-DNA polymer with an excess of a 9 nt complementary DNA strand was 27 °C, when measured in a Tris-acetate-EDTA buffer that contained 12.5 mM Mg^{2+} (Supplementary Fig. 16 and Supplementary Table 8).

The negatively charged APPV-DNA polymer is well dispersed when applied to a mica surface. A typical high-resolution AFM image shows flexible polymers with various lengths that range from 20 nm to more than 200 nm (Fig. 2a). This corresponds to degrees of polymerization of 30 and 301, respectively (Supplementary Fig. 17). The polymers have a common height of 1.5 nm, which corresponds well to ssDNA. The calculated width of the polymer with 9 nt DNA strands that extend to each side of the backbone is 10–15 nm and, taking tip broadening into account, this corresponds well with the observed 15–20 nm (ref. 32).

In addition to nanoscale imaging, advanced AFM methods also enable a detailed mechanical and surface potential characterization of the polymer. As demonstrated in Fig. 2b, the quantitative nanomechanical mapping can simultaneously record morphology and stiffness maps[33]. The Young's modulus of the APPV-DNA polymer was determined to be 9.1 ± 2.4 GPa (Fig. 2b and Supplementary Fig. 17). The flexible polymer is thus much softer than other 1D conductive nanomaterials, such as gold nanowires and carbon nanotubes. For the surface potential measurements, electrostatic force microscopy is able to differentiate the work function of surfaces at the nanoscale. Figure 2c shows a 2D map of the surface potential, which is a fundamental characteristic that represents the conductivity of material interfaces[34,35]. The 2D surface-potential map shows a higher (more negative) potential region compared with the silicon-oxide substrate, which is assigned to the polymer. The potential measurement was exerted during high-resolution imaging, and was determined to be −130 mV (presented in the right panel of Fig. 2c). This implies that the capability of charge transfer at the interface of APPV-DNA is significantly better than those for DNA itself and for silicon oxide (Supplementary Fig. 19). However, the surface potential is still significantly lower than that of gold nanowires and carbon nanotubes.

Immobilization of the polymer on DNA origami

For programmable routing of the polymer we used a rectangular DNA origami and designed patterns of extended DNA staple strands that are complementary to the 9 nt strands on the polymer. The extended DNA strands on the origami are spaced apart approximately by 5 nm. The origami structure was formed according to standard annealing procedures and characterized by AFM (Supplementary Fig. 20). The ssDNA extensions are either not observed or are visible as a band of faint dots by AFM as a result of the flexibility of ssDNA[36]. An origami structure that contains a U-shaped line of staple-strand extensions was applied to a mica surface at room temperature (r.t.) and immediately thereafter an excess of the polymer was added (Fig. 3a). AFM of the resulting structure adsorbed on mica clearly showed a U-shaped protrusion that followed the path of the ssDNA extensions on the origami (Fig. 3a,b, right). The polymer was also assembled on origami that contained linear and 90° curved lines of staple-strand extensions (Fig. 3b). For several of the structures the polymer extends from the origami onto the mica surface. The interaction of the polymer with the origami is sequence specific because the polymer did not bind to an additional parallel line of non-complementary ssDNA extensions (Supplementary Fig. 20). In all three examples the binding yields are high (Fig. 3b). One striking feature observed for the 90° curve structures shown in Fig. 3b is that the polymer is capable of linking two origami structures together by extending from one origami to the other. This is only observed for edges at which end-to-end helix interactions of the origami structures are possible. Surface potential measurements of polymer–origami hybrids in different patterns were carried out by

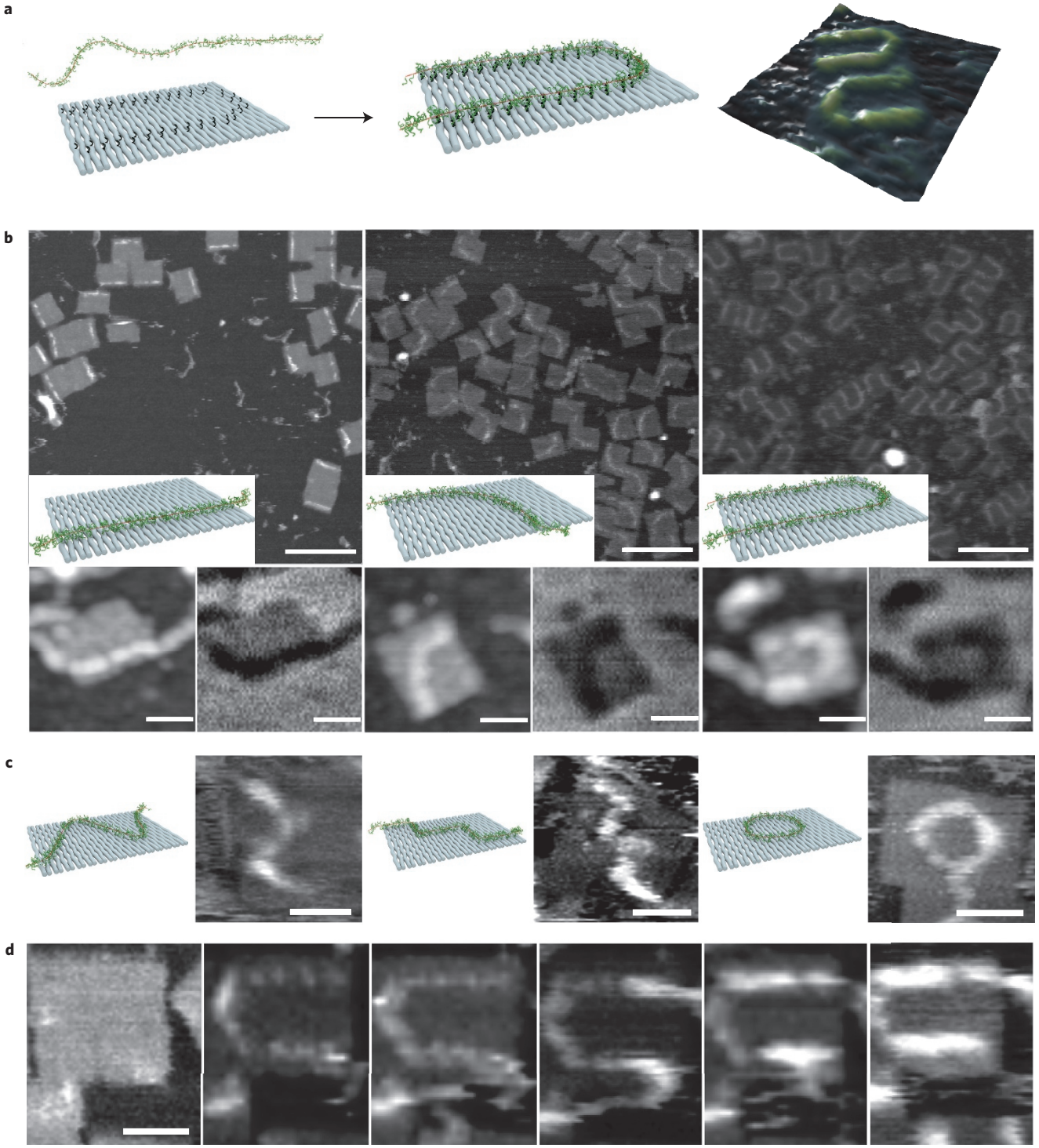

Figure 3 | Immobilization of the APPV-DNA polymer on origami by hybridization of the 9 nt DNA sequences extending from the polymer to patterns of ssDNA extending from the origami. a, Illustration of origami design with a U-shaped pattern of staple-strand extensions and polymer binding to the origami; right, 3D AFM image of two origami structures with polymers assembled on the U-shaped pattern. **b**, Top, AFM topography image of linear, 90° curve and U-shape origami–polymer hybrids; scale bars, 200 nm. Origami designs with the polymer are shown as insets. Bottom, topography image and surface potential maps of single linear-shaped, 90° curve and U-shaped origami–polymer hybrids; scale bars, 50 nm. **c**, Illustrations and AFM images of the assembly of the polymer on wave, staircase and circular patterns on the origami; scale bars, 50 nm. **d**, High-speed AFM imaging of the assembly process. The first image is recorded before the addition of the polymer and subsequent scans are recorded after dipping the AFM tip in a solution that contained the polymer and immediately applying the tip to image the same location. Images were recorded in liquid on a mica surface at a speed of 21 s per image with 1–3 minutes between each image; scale bar, 50 nm.

simultaneously recording topography and surface-potential maps (Fig. 3b, lower panels). As shown by the potential maps the polymer possesses a stronger ability of polarization and charge transfer compared with origami. The surface potential of the polymer on origami is similar to the potential measured without origami (Figs 2c and 3b, and Supplementary Fig. 19).

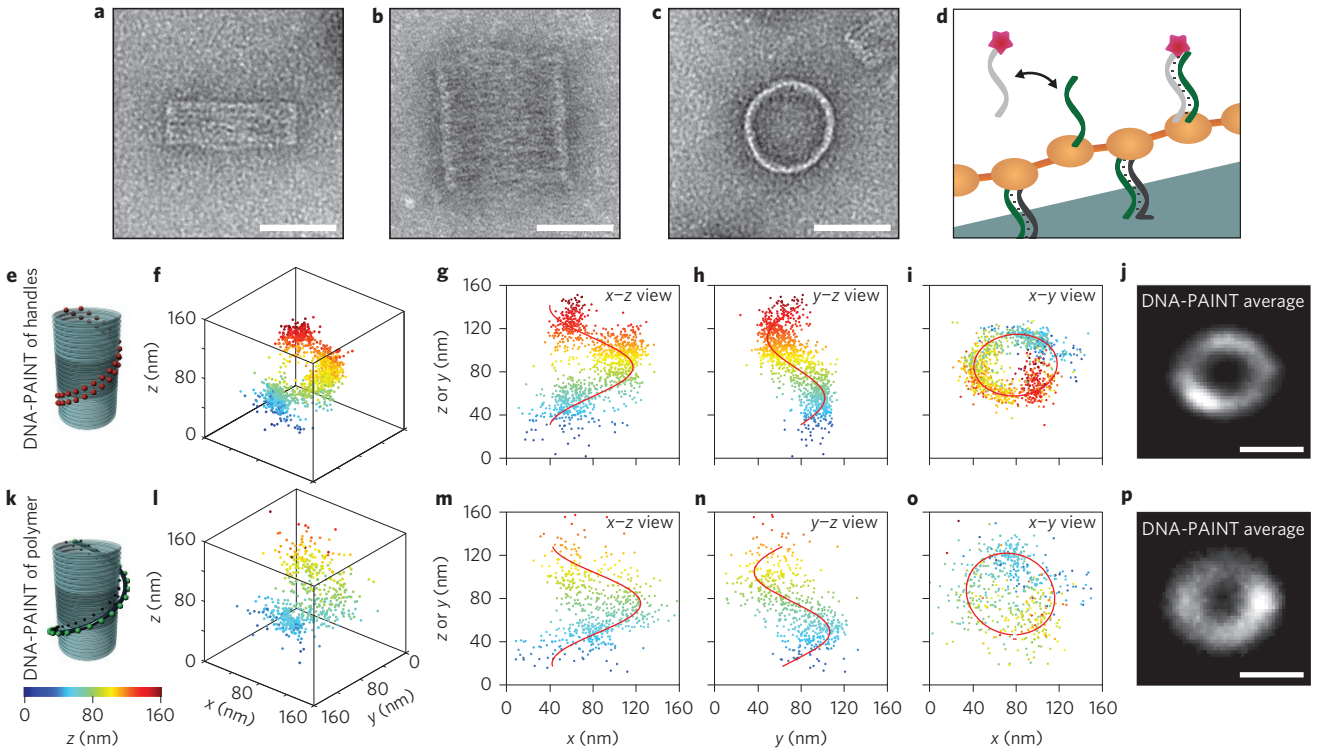

Figure 4 | 3D DNA-PAINT super-resolution imaging of the APPV-DNA polymer immobilized on a 3D DNA nanostructure. a–c, TEM images of cylindrical 3D DNA origami structure; scale bars, 50 nm. **a**, Side view (*x*–*z* plane) of the monomer. **b**, Side view (*x*–*z* plane) of the trimer. **c**, Top view (*x*–*y* plane) of the monomer. **d**, Attachment of the polymer to the DNA structure and DNA-PAINT imaging principle: extended staple strands on the origami (dark grey) are used to immobilize the polymer using complementary strands (green). The excess DNA strands on the DNA-APPV polymer that do not bind to the DNA nanostructure are available as DNA-PAINT docking strands. Fluorescently labelled strands (light grey with pink star) can bind transiently to these docking strands. **e–j**, 3D DNA-PAINT of guide staple strands on the DNA structure. **e**, Schematic illustration of the DNA structure with handle strands (red dots) for DNA-PAINT. **f–i**, Representative 3D DNA-PAINT super-resolution images of a single DNA structure (colour indicates height). Localizations are shown along with the helical fits (red lines). **f**, 3D view. **g**, *x*–*z* view. **h**, *y*–*z* view. **i**, *x*–*y* view. **j**, Class-averaged *x*–*y* views of 137 structures; scale bar, 50 nm. **k**, Schematic illustration of the DNA structure with attached polymer (black). Green dots indicate strands on the polymer available for DNA-PAINT imaging. **l–p**, Representative 3D DNA-PAINT super-resolution images of a single polymer bound to a DNA structure (colour indicates height). **l**, 3D view. **m**, *x*–*z* view. **n**, *y*–*z* view. **o**, *x*–*y* view. **p**, Class-averaged *x*–*y* views of 89 structures; scale bar, 50 nm.

An additional series of three polymer-wiring patterns on wave, staircase and circular staple-strand designs was formed, as shown in Fig. 3c. This series demonstrates the flexibility of the routing of the polymer—especially noticeable is the staircase design in which the polymer is forced to make sharp 90° turns. From the circular structure the excess of the polymer is observed as a line connected to the circle. The yields of assembly of the polymer on these more complex routings were, however, lower than the others (Supplementary Fig. 21).

The mechanism of self-assembly of the polymer on the U-shaped pattern was investigated by high-speed AFM imaging (Fig. 3d and Supplementary Fig. 22). First, an image was recorded that showed the pristine origami. After retracting the tip and dipping it in a solution that contained the polymer, a subsequent scan at the same position of the surface revealed the U-shape polymer structures on the origami. This could be caused either by interactions between polymers immobilized on the AFM tip and the ssDNA staple extensions or by fast immobilization of very short oligomers on the path. In turn, two polymers attach at each end of the U-shaped path and gradually cover a larger part of the path. We suggest that this occurs via a mechanism by which the polymers zip up with the path. Only the part of the polymer that is immobilized on the surface can be observed by AFM. At the end of the short sequence shown in Fig. 3d, the U shape is partly covered by the polymer. However, in most of the structures shown in Fig. 3b and Supplementary Fig. 23 the origami appears to be covered fully by the polymer. It is striking that the polymer continuously follows the full path on the majority of origami structures without forming bulges or half-filled paths. Although several of the polymers are sufficiently long to cover a full U pattern, in many cases it may also be covered by two or more shorter polymers that overlap; that is, there are places on the path that bind two polymers. This also seems to be consistent with the variation in the polymer width on the origami surface.

The addressability of the DNA origami makes it possible to co-immobilize other materials and study the interaction with the polymer. For this purpose we observed the Förster resonance energy transfer (FRET) between the polymer and a single Alexa 647 acceptor attached on one of the origami staple strands that binds to the polymer (Supplementary Fig. 15). In the presence of the polymer at the origami a 20× enhancement of the emission of the acceptor was observed.

Routing and imaging of the polymer in 3D

DNA origami also allows folding in 3D and a variety of nanostructures that range from hollow to solid shapes have been reported[37,38]. Here we want to demonstrate that such structures are applicable for creating a predesigned path for a 3D routing of the polymer. For this purpose we designed a cylindrical DNA structure that consists of stacked rings of double helices. The cylinder is assembled from three concentric layers of helices connected via extended staple strands, with a hexagonal cross-section. The long origami scaffold runs through only the outer and middle layers, and scaffold parity strands for the inner layer consist of short synthetic oligonucleotides.

Three unique monomers, each folded from a single scaffold, are linked coaxially with staple strands in a two-step assembly process. The final trimer has a height of approximately 100 nm and an outer diameter of approximately 60 nm, and consists of ~36 kilobase pairs of DNA (M_W ~23.8×10^7 Da). Transmission electron microscopy (TEM) images of the monomer and the trimer cylinder are shown in Fig. 4a–c and a detailed model of the structure is given in Supplementary Fig. 24. The increase in the apparent diameter of the cylinders in the side TEM profiles (Fig. 4a,b) to ~90 nm from the predicted 60 nm, as seen in the top profile (Fig. 4c), is the result of collapse after drying, an artefact often observed during negative staining of hollow objects.

AFM characterization of a soft 3D structure (such as the routed polymer on the origami) is challenging because of the relatively high forces applied to the structure image acquisition (tip–sample interaction). In addition, the polymer does not provide sufficient contrast in a negative-stain TEM.

To achieve a 3D characterization of the polymer routed in 3D on a DNA origami structure, we used DNA-PAINT, a super-resolution fluorescence microscopy technique. DNA-PAINT allows minimally invasive imaging of fragile 3D nanostructures in their native environment with sub 10 nm lateral and sub 30 nm axial resolution. DNA-PAINT is based on the transient binding of fluorescently labelled short DNA imager strands to complementary docking strands attached to a target. These repeating and specific binding events produce an apparent blinking at the target site and enable super-resolution imaging[39–41]. 3D information can be obtained by shaping the emission profile of the fluorescence signal of single molecules that depend on their relative axial position to the focal plane of the objective[42,43].

Figure 4d shows a schematic representation of the DNA-PAINT imaging process of the polymer bound to a DNA structure. The excess DNA strands on the APPV-DNA polymer that do not bind to the DNA nanostructure are available as DNA-PAINT docking strands. The DNA structure itself is 'labelled' with two parallel rows of staple-strand extensions on the outside to form a 360° right-handed helical pattern (Fig. 4e). In a first imaging experiment, we used DNA-PAINT to visualize this helical staple-strand pattern in 3D. This was achieved by immobilization of the biotinylated origami on a streptavidin-coated glass slide (see the Supplementary Information), followed by 3D super-resolution imaging using DNA imager strands complementary to the staple-strand extensions on the DNA structure. Figure 4f shows the resulting 3D DNA-PAINT super-resolution image (colour indicates height) of a single DNA nanostructure. The right-handed helix in the DNA-PAINT image corresponds well to the designed pattern (Fig. 4e) (see also Supplementary Movie 1). Three 2D projections of the localizations from Fig. 4f along with the respective fits to the data (see the Supplementary Information for details about the fitting process) are shown in Fig. 4g–i, and underline the mathematically correct shape of the helix. In addition to the single-particle measurement, we performed electron microscopy-style averaging of 137 structures in the x–y plane (Fig. 4j) and determined the diameter and width of the projection to 53 ± 2 nm and 15 ± 1 nm (mean ± s.d.). These parameters were determined by fitting double Gaussian distributions to eight line profiles through the centre of the ring and then calculating their average distances and full-width at half-maximum (FWHM). Under the imaging conditions used, we localized single-molecule events in 2D with a precision of approximately 5 nm, and thus theoretically obtained an imaging resolution of approximately 12 nm. The measured width of the ring-like projection of 15 nm supports the high rigidity and yield of the 3D DNA nanostructure.

For 3D DNA-PAINT imaging of the polymer, the surface-immobilized DNA nanostructure was incubated with the APPV-DNA polymer to allow it to bind to the structure, as illustrated in Fig. 4k. The guiding staple-strand extensions are complementary to the strands on the polymer and hence 'route it' to the helical structure. The final assembled hybrid was then imaged using DNA-PAINT probes that are complementary (that is, have the same sequence as the guide extensions) to the DNA strands on the polymer (Fig. 4d). Figure 4l shows the resulting 3D DNA-PAINT super-resolution image (colour indicates height) of the polymer on a single DNA nanostructure. Figure 4m–o shows the same projections as in Fig. 4g–i. Similar to the direct imaging of the DNA nanostructure, the polymer follows the helical shape of the guide staple strands in 3D (see also Supplementary Movie 2). As in the direct nanostructure-imaging case, we here localized single-molecule events in 2D with a precision of approximately 5 nm, and thus theoretically obtained an imaging resolution of approximately 12 nm. The analysis of the class average in Fig. 4p ($n = 89$) yields a diameter of 52 ± 3 nm and FWHM of 22 ± 2 nm (mean ± s.d.). Again, these values are in good agreement with the designed distances. The increased FWHM can be explained by the 'added' flexibility of the attached polymer. The DNA-PAINT imager strands do not interact with the guide strands on the DNA structure because they have orthogonal sequences.

Conclusions

The essence of nanotechnology is to manipulate matter at the nanoscale, and here we present the first method to control the immobilization and routing of linear polymers that otherwise lack the ability to undergo programmed self-assembly. By modifying the APPV polymer with short DNA strands that extend with high density along the polymer backbone we enabled the programmed self-assembly of the polymer into a variety of designed paths in 2D and 3D DNA nanostructures. The DNA sequences, furthermore, allowed the characterization in 3D by DNA-PAINT super-resolution microscopy.

The APPV polymers have a π-conjugated backbone, and they display a range of electronic properties and are electroluminescent[44]. Hence, this method can open up intriguing possibilities to connect molecular circuitry electronically. It has been shown that DNA origami structures immobilize onto specific patterns created by e-beam lithography on a silicon-oxide surface[45]. Potentially, the formation of such patterns between electrodes could provide electronic contacts to specific sites of the origami structure. Moreover, as this technique is not limited to 2D, it has the potential to create very compact 3D electronics.

The method also opens the way for studies and applications of the optical properties of such polymers, as we have shown that the absorption and emission of the conjugated polymer backbone are intact after it has been modified with DNA and that it can interact with a co-immobilized acceptor dye. Hence, this paves the way for studies of the relation between conformation and optical properties and the interaction with other optical materials immobilized at specific positions at the DNA origami, such as organic dyes, nanoparticles and quantum dots.

The synthetic protocol described here is principally extendable to all linear polymers that can be prepared with hydroxyl-containing side chains and are compatible with automated DNA synthesis. We demonstrate here that equipping polymers with DNA sequences in a brush-type fashion provides a unique method for controlling the shape of individual polymers and potentially exploit their properties.

Methods

Methods and any associated references are available in the online version of the paper.

Received 13 February 2015; accepted 22 July 2015;
published online 31 August 2015

References

1. Heeger, A. J. Semiconducting and metallic polymers: the fourth generation of polymeric materials. *Synthetic Met.* **125,** 23–42 (2001).

2. Heeger, A. J. Semiconducting polymers: the third generation. *Chem. Soc. Rev.* **39,** 2354–2371 (2010).
3. Facchetti, A. π-Conjugated polymers for organic electronics and photovoltaic cell applications. *Chem. Mater.* **23,** 733–758 (2011).
4. Baeg, K.-J. *et al.* High speeds complementary integrated circuits fabricated with all-printed polymeric semiconductors. *J. Polym. Sci. B* **49,** 62–67 (2011).
5. Gong, S., Yang, C. & Qin, J. Efficient phosphorescent polymer light-emitting diodes by suppressing triplet energy back transfer. *Chem. Soc. Rev.* **41,** 4797–4807 (2012).
6. Zheng, H. *et al.* All-solution processed polymer light-emitting diode displays. *Nature Commun.* **4,** 1–7 (2013).
7. Günes, S., Neugebauer, H. & Sariciftci, N. S. Conjugated polymer-based organic solar cells. *Chem. Rev.* **107,** 1324–1338 (2007).
8. Thomas, S. W., Joly, G. D. & Swager, T. M. Chemical sensors based on amplifying fluorescent conjugated polymers. *Chem. Rev.* **107,** 1339–1386 (2007).
9. Barbara, P. F., Gesquiere, A. J., Park, S. J. & Lee, Y. J. Single-molecule spectroscopy of conjugated polymers. *Acc. Chem. Res.* **38,** 602–610 (2005).
10. Hugel, T. *et al.* Single-molecule optomechanical cycle. *Science* **296,** 1103–1106 (2002).
11. Kawai, S. *et al.* Quantifying the atomic-level mechanics of single long physisorbed molecular chains. *Proc. Natl Acad. Sci. USA* **111,** 3968–3972 (2014).
12. Taniguchi, M. *et al.* Self-organized interconnect method for molecular devices. *J. Am. Chem. Soc.* **128,** 15062–15063 (2006).
13. Lafferentz, L. *et al.* Conductance of a single conjugated polymer as a continuous function of its length. *Science* **323,** 1193–1197 (2009).
14. Shimomura, T. *et al.* Conductivity measurement of insulated molecular wire formed by molecular nanotube and polyaniline. *Synthetic Met.* **153,** 497–500 (2005).
15. Kiriy, A. *et al.* Cascade of coil–globule conformational transitions of single flexible polyelectrolyte molecules in poor solvent. *J. Am. Chem. Soc.* **124,** 13454–13462 (2002).
16. Shimomura, T., Akai, T., Abe, T. & Ito, K. Atomic force microscopy observation of insulated molecular wire formed by conducting polymer and molecular nanotube. *J. Chem. Phys.* **116,** 1753–1756 (2002).
17. Ouchi, M., Badi, N., Lutz, J.-F. & Sawamoto, M. Single-chain technology using discrete synthetic macromolecules. *Nature Chem.* **3,** 917–924 (2011).
18. Müllen, K. Evolution of graphene molecules: structural and functional complexity as driving forces behind nanoscience. *ACS Nano* **8,** 6531–6541 (2011).
19. Palma, C.-A. & Samori, P. Blueprinting macromolecular electronics. *Nature Chem.* **3,** 431–436 (2011).
20. Lörtscher, E. Wiring molecules into circuits. *Nature Nanotech.* **8,** 381–384 (2013).
21. Peng, H., Zhang, L., Soeller, C. & Travas-Sejdic, J. Conducting polymers for electrochemical DNA sensing. *Biomaterials* **30,** 2132–2148 (2009).
22. Lo, P. K. & Sleiman, H. F. Nucleobase-templated polymerization: copying the chain length and polydispersity of living polymers into conjugated polymers. *J. Am. Chem. Soc.* **131,** 4182–4183 (2009).
23. Rothemund, P. W. K. Folding DNA to create nanoscale shapes and patterns. *Nature* **440,** 297–302 (2006).
24. Tørring, T., Voigt, N. V., Nangreave, J., Yan, H. & Gothelf, K. V. DNA origami: a quantum leap for self-assembly of complex structures. *Chem. Soc. Rev.* **40,** 5636–5646 (2011).
25. Sacca, B. & Niemeyer, C. M. Functionalization of DNA nanostructures with proteins. *Chem. Soc. Rev.* **40,** 5910–5921 (2011).
26. Wang, Z. G. & Ding, B. Engineering DNA self-assemblies as templates for functional nanostructures. *Acc. Chem. Res.* **47,** 1654–1662 (2014).
27. Maune, H. T. *et al.* Self-assembly of carbon nanotubes into two-dimensional geometries using DNA origami templates. *Nature Nanotech.* **5,** 61–66 (2010).
28. Chaix, C., Minard-Basquin, C., Delair, T., Pichot, C. & Mandrand, B. Oligonucleotide synthesis on maleic anhydride copolymers covalently bound to silica spherical support and characterization of the obtained conjugates. *J. Appl. Polym. Sci.* **70,** 2487 (1998).
29. Henckens, A., Duyssens, I., Lutsen, L., Vanderzande, D. & Cleij, T. J. Synthesis of poly(*p*-phenylene vinylene) and derivatives via a new precursor route, the dithiocarbamate route. *Polymer* **47,** 123–131 (2006).
30. Vandenbergh, J. *et al.* Synthesis and characterization of water-soluble poly(*p*-phenylene vinylene) derivatives via the dithiocarbamate precursor route. *Eur. Polym. J.* **47,** 1827–1835 (2011).
31. Minard-Basquin, C., Chaix, C., Pichot, C. & Mandrand, B. Oligonucleotide –polymer conjugates: effect of the method of synthesis on their structure and performance in diagnostic assays. *Bioconjugate Chem.* **11,** 795–805 (2000).
32. Volcke, C. *et al.* Influence of DNA condensation state on transfection efficiency in DNA/polymer complexes: an AFM and DLS comparative study. *J. Biotechnol.* **125,** 11–21 (2006).
33. Zhang, S. *et al.* Coexistence of ribbon and helical fibrils originating from $hIAPP_{20–29}$ revealed by quantitative nanomechanical atomic force microscopy. *Proc. Natl Acad. Sci. USA* **110,** 2798–2803 (2013).
34. Pfeffer, C. *et al.* Filamentous bacteria transport electrons over centimetre distances. *Nature* **491,** 218–221 (2012).
35. Sinensky, A. K. & Belcher, A. M. Label-free and high-resolution protein/DNA nanoarray analysis using Kelvin probe force microscopy. *Nature Nanotech.* **2,** 653–659 (2007).
36. Ke, Y., Lindsay, S., Chang, Y., Liu, Y. & Yan, H. Self-assembled water-soluble nucleic acid probe tiles for label-free RNA hybridization assays. *Science* **319,** 180–183 (2008).
37. Shih, W. M. & Lin, C. Knitting complex weaves with DNA origami. *Curr. Opin. Chem. Biol.* **20,** 276–282 (2010).
38. Douglas, S. M. *et al.* Self-assembly of DNA into nanoscale three-dimensional shapes. *Nature* **459,** 414–418 (2009).
39. Iinuma, R. *et al.* Polyhedra self-assembled from DNA tripods and characterized with 3D DNA-PAINT. *Science* **344,** 65–69 (2014).
40. Jungmann, R. *et al.* Multiplexed 3D cellular super-resolution imaging with DNA-PAINT and Exchange-PAINT. *Nature Methods* **11,** 313 (2014).
41. Jungmann, R. *et al.* Single-molecule kinetics and super-resolution microscopy by fluorescence imaging of transient binding on DNA origami. *Nano Lett.* **10,** 4756–4761 (2010).
42. Kao, H. P. & Verkman, A. S. Tracking of single fluorescent particles in three dimensions: use of cylindrical optics to encode particle position. *Biophys. J.* **67,** 1291–1300 (1994).
43. Huang, B., Wang, W., Bates, M. & Zhuang, X. Three-dimensional super-resolution imaging by stochastic optical reconstruction microscopy. *Science* **319,** 810–813 (2008).
44. Burns, P. L. *et al.* Chemical tuning of the electronic properties of poly(*p*-phenylenevinylene)-based copolymers. *J. Am. Chem. Soc.* **115,** 10117–10124 (1993).
45. Kershner, R. J. *et al.* Placement and orientation of individual DNA shapes on lithographically patterned surfaces. *Nature Nanotech.* **4,** 557–561 (2009).

Acknowledgements

We thank P.W.K. Rothemund for discussions. This work was funded by the Danish National Research Foundation (Centre for DNA Nanotechnology, DNRF81), Sino-Danish Centre for Education and Research, Carlsberg Foundation, Danish Research Council (V.B.) (Sapere Aude Starting Grant (A.N.Z. and V.B.), STENO grant and an individual post-doctorate grant (R.O.)), Villum Foundation (Young Investigator Program (M.D.)), and the Lundbeck Foundation (A.N.Z). R.J. acknowledges support from the Deutsche Forschungsgemeinschaft through the Emmy Noether program (DFG JU 2957/1–1) and the Max Planck Society. W.M.S. acknowledges support for the contributions to his laboratory from the National Science Foundation (CCF-1317291), Army Research Office (W911NF-12-1-0420) and the Wyss Institute for Biologically Inspired Engineering.

Author contributions

J.B.K. and M.M. synthesized and characterized the APPV-DNA polymer. L.L., J.S., Q.L. and J.V. conducted the SPM experiments. A.L.B.K. and A.K. designed the DNA origami and conducted the AFM experiments. A.A.A.S. and A.N.Z. assisted in performing and interpreting the GPC analysis. R.O. performed XPS and assisted in the interpretation. D.G. measured the fluorescence quantum yields of the polymer. M.M. designed and conducted the FRET experiments. J.B.W., R.J., S.F.J.W., W.M.S. and K.V.G. designed the DNA-PAINT experiments. S.F.J.W. and W.M.S. designed the 3D DNA origami samples, and S.F.J.W. assembled, purified and characterized the 3D DNA origami samples. J.B.W., M.T.S. and F.S. performed the DNA-PAINT experiments and analysed the data. M.T.S. wrote the 3D image analysis and fitting software. R.J. performed the class averaging. P.Y. and R.J. supervised the DNA-PAINT study. A.Z., V.B. and F.B. supervised parts of the project. M.D. supervised and analysed the SPM experiments. K.V.G. conceived and supervised the project. J.B.K., M.D., S.F.J.W., A.L.B.K., J.B.W., M.T.S., R.J. and K.V.G. wrote the paper.

Additional information

Supplementary information is available in the online version of the paper. Reprints and permissions information is available online at www.nature.com/reprints. Correspondence and requests for materials should be addressed to M.D. and K.V.G.

Competing financial interests

The authors declare no competing financial interests.

Methods

For the poly(APPV-DNA) synthesis, monomer **3** was polymerized according to a known procedure[23].The resulting APPV-TBDPS polymer (**4a**) in THF (22 ml, 3.4 mg ml^{-1}) was partly deprotected in HF–pyridine (11 mmol HF, 75 equiv.). The mixture was stirred at r.t. for 90 minutes to provide polymer **4b**. Synthesis of the DNA-coated APPV polymer was performed on a MerMade 12 oligonucleotide synthesizer. Polymer **4b** (7 mg) was dissolved in anhydrous $CHCl_3$ (4 ml) and added with an activator to a dT-functionalized CPG3000 column pre-functionalized as a phosphoramidite. Subsequently, tetra-*n*-butylammonium fluoride in THF (1 M) was added to the column. DNA was synthesized by phosphoramidite chemistry from the hydroxyl groups on the polymer. After standard deprotection and cleavage from the solid support, the polymer was purified by size-exclusion chromatography PD-10 columns packed with Sepharose CL-2B using triethylamine/acetate buffer(50 mM, pH 7) as the eluent. The polymer was characterized by GPC, gel electrophoresis (0.4% agarose), XPS, UV-vis, fluorescence spectroscopy and AFM. DNA origami was prepared as described previously and selected staple strands were extended with 12 nt ssDNA including a $(T)_3$ spacer[18,19]. The quantitative nanomechanical mapping was operated with a commercial Multimode VIII SPM controller (Bruker). Surface potential measurements were performed on an AFM (Multimode VIII, Bruker) with a Co/Cr-coated tip (MESP). For the DNA-PAINT imaging, the sample was prepared by immobilization of the biotinylated DNA structure on streptavidin–biotin-labelled BSA-covered glass slides in a flow chamber and imaged as previously described[39]. Super-resolution reconstruction was performed using the N-STORM package and a custom MATLAB software.